

## Dispersion-scan characterization of partially coherent ultrashort pulses: a differential evolution algorithm analysis

YIN Chen, YANG Pei-long, MEI Chao

Citation:

YIN Chen, YANG Pei-long, MEI Chao. Dispersion-scan characterization of partially coherent ultrashort pulses: a differential evolution algorithm analysis[J]. *Chinese Optics*, In press. doi: 10.37188/CO.EN-2026-0001

尹琛, 杨佩龙, 梅超. 部分相干超短脉冲的色散扫描表征: 基于差分进化算法的分析[J]. *中国光学*, 优先发表. doi: 10.37188/CO.EN-2026-0001

View online: <https://doi.org/10.37188/CO.EN-2026-0001>

### Articles you may be interested in

#### [Short pulse laser drive technology in a distance-selective imaging system](#)

距离选通成像系统中短脉冲激光驱动技术研究

*Chinese Optics*. 2023, 16(3): 567 <https://doi.org/10.37188/CO.2022-0142>

#### [Optimization design method for counter-rotating prisms atmospheric dispersion corrector](#)

旋转式大气色散校正器的优化设计方法

*Chinese Optics*. 2025, 18(4): 859 <https://doi.org/10.37188/CO.2024-0204>

#### [Measurement of methane concentration with wide dynamic range using heterodyne phase-sensitive dispersion spectroscopy](#)

基于外差相敏色散光谱技术的宽动态范围甲烷气体检测

*Chinese Optics*. 2024, 17(4): 789 <https://doi.org/10.37188/CO.2023-0177>

#### [Flatness detection method of splicing detector based on channel spectral dispersion](#)

基于通道光谱色散的拼接探测器平整度检测方法

*Chinese Optics*. 2025, 18(4): 889 <https://doi.org/10.37188/CO.EN-2024-0026>

#### [Fabric image retrieval algorithm based on fractal coding and Zernike moment under the wavelet transform](#)

小波变换下基于分形编码和 Zernike 矩的织物图像检索算法

*Chinese Optics*. 2023, 16(3): 715 <https://doi.org/10.37188/CO.EN-2022-0021>

#### [Recent progress on synthesis and optical characterization of two-dimensional Bi<sub>2</sub>O<sub>2</sub>Se](#)

二维Bi<sub>2</sub>O<sub>2</sub>Se的制备与光学表征研究进展

*Chinese Optics*. 2023, 16(1): 24 <https://doi.org/10.37188/CO.2022-0071>

文章编号 2097-1842(xxxx)x-0001-12

## Dispersion-scan characterization of partially coherent ultrashort pulses: a differential evolution algorithm analysis

YIN Chen<sup>1</sup>, YANG Pei-long<sup>2\*</sup>, MEI Chao<sup>1\*</sup>

(1. Department of Physics, School of Physical Science and Technology, Ningbo University,  
Ningbo 315211, P.R. China;

2. Laboratory of Infrared Materials and Devices, The Research Institute of Advanced Technologies,  
Ningbo University, Ningbo 315211, P.R. China)

\* Corresponding author, E-mail: yangpeilong@nbu.edu.cn; meichao@nbu.edu.cn

**Abstract:** Objective: To retrieve the pulse information from the dispersion scanning (d-scan) trace, a differential evolution (DE) algorithm is used. Methods: A partially coherent pulse train is generated and then test by traditional DE algorithm and its improved version. Results: The errors retrieved using the traditional and improved DE algorithms are 7% and 1%, respectively. Conclusion: The improved algorithm can more accurately retrieve the d-scan trace of partially coherent pulse train.

**Key words:** ultrashort pulse characterization; dispersion scan; differential evolution algorithm

## 部分相干超短脉冲的色散扫描表征：基于差分进化算法的分析

尹琛<sup>1</sup>, 杨佩龙<sup>2\*</sup>, 梅超<sup>1\*</sup>

(1. 宁波大学物理科学与技术学院, 浙江宁波 315211;

2. 宁波大学高等研究院, 浙江宁波 315211)

**摘要:**目的: 为了从色散扫描轨迹中恢复脉冲信息, 本文采用了一种差分进化算法。方法: 生成一个部分相干脉冲序列, 并使用传统差分进化算法及其改进版本进行测试。结果: 传统差分进化算法和改进差分进化算法的恢复误差分别为 7% 和 1%。结论: 改进算法能够更准确地恢复部分相干脉冲序列的色散扫描轨迹。

**关键词:** 超短脉冲表征; 色散扫描; 差分进化算法

中图分类号: TP394.1; TH691.9 文献标志码: A doi: 10.37188/CO.EN-2026-0001 CSTR: 32171.14.CO.EN-2026-0001

收稿日期: 2026-01-05; 修订日期: xxxx-xx-xx

基金项目: 中文基金

This work was supported in part by the National Natural Science Foundation of China under (No. 62275015, No. 62205015).

## 1 Introduction

Ultrafast optical science has long relied on the assumption of pulse-to-pulse stability and coherence. Techniques ranging from chirped-pulse amplification<sup>[1]</sup> to frequency-resolved optical gating<sup>[2]</sup> are fundamentally designed around the existence of a reproducible, coherent electric field. This paradigm of perfect coherence has enabled breakthroughs in high-field physics<sup>[3-4]</sup>, time-resolved spectroscopy<sup>[5-6]</sup>, and precision metrology<sup>[7-8]</sup>. However, emerging experimental evidence increasingly challenges this idealization, showing that many ultrafast sources exhibit significant stochastic variations<sup>[9-11]</sup>. Such fluctuations, often described as partial coherence or pulse instability, are not merely noise but arise intrinsically from the dynamical behavior of diverse laser systems.

The origins of pulse train instability are varied and often inherent to the laser mechanism. Free-electron lasers operating in self-amplified spontaneous emission mode, for instance, naturally produce pulses with large fluctuations in amplitude and phase<sup>[12-13]</sup>. Similarly, conventional gain media including Ti:sapphire solid-state lasers<sup>[14]</sup>, fiber amplifiers<sup>[15]</sup>, semiconductor lasers<sup>[16]</sup>, and dye systems<sup>[17]</sup> can exhibit imperfect mode-locking or nonlinear dynamics that lead to stochastic pulse variations. The resulting pulse trains suffer from degraded inter-pulse coherence, with randomized phase relationships between successive pulses. This instability has profound practical consequences. In coherent control experiments, it disrupts interference-based schemes<sup>[18]</sup>. In pump-probe spectroscopy, timing jitter and pulse-shape variations blur transient signals and obscure kinetic information<sup>[19]</sup>. Perhaps most critically, conventional diagnostic tools designed for stable pulses can yield dangerously misleading results. For example, an autocorrelator may interpret a fluctuating pulse structure as a smooth, transform-limited pulse of shorter duration, thereby com-

pletely concealing the underlying instability<sup>[20]</sup>.

As ultrafast technology advances toward shorter pulses, broader spectra, and novel laser architectures, the likelihood of encountering partially coherent operation increases. There is thus a pressing need for characterization methods that are not only functional under ideal conditions but are explicitly designed to detect, quantify, and disentangle the effects of partial coherence. An effective technique must fulfill two essential criteria. First, it must be sensitive enough to identify the presence of instability; second, its retrieval algorithm must be robust and general enough to model the stochastic nature of the source without imposing unrealistic constraints of perfect coherence.

The dispersion-scan (d-scan) technique has emerged as a powerful and versatile tool for characterizing ultrashort pulses, particularly in the single and few-cycle regimes<sup>[21-23]</sup>. By recording a spectrally resolved nonlinear signal, typically second-harmonic generation, as a function of applied dispersion, d-scan offers a simple experimental setup, immunity to spatial averaging effects, and direct sensitivity to spectral phase. Its reliability has been well established for stable, coherent pulses across a wide range of energies and wavelengths<sup>[24]</sup>. However, its performance in the presence of pulse-train instability remains an open question. It is unclear whether the d-scan trace of a partially coherent source differs systematically from that of a stable source. A central challenge lies in the fact that standard phase-retrieval algorithms, which assume a single deterministic pulse shape, are not readily adaptable for extracting meaningful statistical information from an ensemble of fluctuating pulses.

This work addresses these issues by systematically investigating the interplay between partial coherence and the d-scan measurement process. Moving beyond the simple question of whether d-scan remains applicable, we examine how specific forms of pulse instability, particularly variations in spectral width and shape, manifest as distinctive signa-

tures in the d-scan signal space. We demonstrate that the d-scan trace encodes information about the underlying pulse statistics, which can be decoded using an appropriately generalized retrieval algorithm.

To achieve this, we depart from traditional gradient-based phase retrieval and adopt a global optimization approach based on differential evolution (DE)<sup>[25-27]</sup>. DE is a population-based stochastic optimizer known for its ability to handle non-differentiable, multimodal, and noisy objective functions, making it well-suited to the challenges of fitting models to data from unstable sources. We develop a retrieval framework in which the algorithm searches not for a single pulse shape, but for parameters that describe the statistical distribution of pulses. Furthermore, we compare the performance of traditional DE and an improved variant under conditions of varying spectral width and shape, offering insight into their respective strengths and limitations in the context of partially coherent pulse characterization.

## 2 Preparation of pulse trains, dispersion scan and algorithm

### 2.1 Generation of partially coherent pulse trains

Before applying the DE algorithm to retrieve unstable pulse trains, it is necessary to generate physically reasonable partially coherent pulse ensembles. Since the phase between consecutive pulses should vary significantly, we adopt the random-phase method proposed by T. Pfeifer *et al.*<sup>[28]</sup>. This numerical approach iteratively adjusts the spectral phase in each loop, enabling the generation of pulse trains with controlled stochastic behavior. The method starts from the average spectral intensity  $I(\omega)$ . The electric field in the frequency domain is expressed as  $E_0(\omega) = A_0(\omega)\exp[i\varphi(\omega)]$  with a spectral phase  $\varphi_0(\omega)$  and the spectral amplitude  $A_0(\omega)=[I(\omega)]^{1/2}$ . Initially, a discrete random spectral phase  $\varphi_0(\omega)$  is generated by assigning independent

random numbers uniformly distributed between  $-\pi$  and  $\pi$  at each sampled frequency  $\omega$ . Performing an inverse Fourier transform on the resulting complex spectrum yields an initial temporal electric field  $E_0(t)$ . To incorporate prior knowledge about the average pulse duration,  $E_0(t)$  is multiplied by a temporal amplitude filter  $G(t)$ , whose width corresponds to the target average pulse duration. The shape of  $G(t)$  should match the expected average temporal waveform. Due to the random initialization of the spectral phase, the filtered temporal field  $E(t) = E_0(t)G(t)$  varies from pulse to pulse, yet the ensemble of generated pulses collectively satisfies the prescribed average duration and spectral shape. The degree of instability within the pulse train is quantified by the interpulse coherence, defined as<sup>[29]</sup>:

$$|g_{12}^{(1)}(\lambda, t_1 - t_2)| = \left| \frac{\langle E_i^*(\lambda, t_1) E_j(\lambda, t_2) \rangle_{i \neq j}}{\sqrt{\langle |E_i(\lambda, t_1)|^2 \rangle \langle |E_i(\lambda, t_1)|^2 \rangle}} \right|, \quad (1)$$

where  $E_i$  and  $E_j$  represent complex spectral amplitudes of two independent pulses in the ensemble, and angular brackets denote ensemble averaging. Here,  $t_1$  and  $t_2$  correspond to the generation times of the spectral pairs, though in practice the delay  $t_1 - t_2$  is often set to zero when only spectral characteristics are considered. For a fully coherent ensemble where all pulses are identical,  $|g_{12}^{(1)}| \equiv 1$ , implying that all pulses are compressible to the same bandwidth-limited duration. We examine two distinct scenarios in the generation process. First, we consider initial spectral amplitudes  $A_0(\omega)$  with hyperbolic secant (HS) profiles of different bandwidths: 30, 60, and 100 THz [full width at half maximum (FWHM) of spectral amplitude]. The corresponding Fourier-transform-limited durations are 23.4 fs, 11.7 fs, and 7 fs, respectively. In this case, an HS-shaped temporal filter with a 20 fs FWHM is applied. Second, we study three different spectral profiles, HS, Gaussian, and super-Gaussian (SG), each with a fixed bandwidth of 60 THz. The temporal filter shape is adjusted to match the expected temporal

waveform of each profile, while its FWHM is kept at 20 fs. These variations in spectral shape are motivated by the realistic instability observed in mode-locked lasers due to fluctuations in lasing dynamics. For each case, an ensemble of 6000 pulses is generated. The average spectral intensity of the ensemble for different initial bandwidths is shown in Fig. 1(a)–(c), where the gray curves represent individual

pulses and the colored dashed lines denote the ensemble average. As expected, the average spectral width increases with the initial bandwidth. The corresponding interpulse coherence, computed via Eq. (1), is plotted in Fig. 1(d). For all three bandwidths, the interpulse coherence remains below 0.04, confirming the generation of a highly incoherent pulse train.

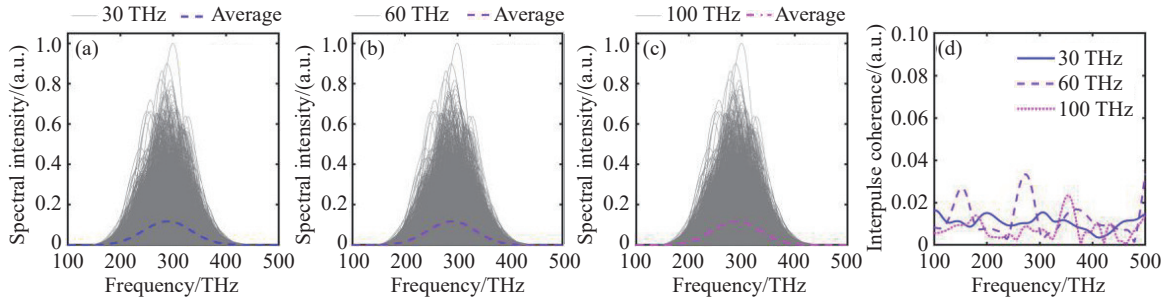


Fig. 1 Partially coherent pulse trains generated with initial spectral FWHM of (a) 30 THz, (b) 60 THz, and (c) 100 THz. Gray curves: 6000 randomly generated pulses. Dashed lines: averaged spectral intensity (blue: 30 THz, violet: 60 THz, magenta: 100 THz). (d) Interpulse coherence for 30 THz (blue solid), 60 THz (violet dashed), and 100 THz (magenta dotted).

The ensemble and average spectra for the three spectral profiles (HS, Gaussian, SG) are displayed in Fig. 2(a)–(c). The spectral width is fixed at 60 THz, and the temporal filter parameters match those used in Fig. 1. Compared with Fig. 1, the resulting spectral widths in Fig. 2 are narrower, which we attribute to the different filter functions employed in the two cases. As shown in Fig. 2(d), the

random-phase method yields a slightly higher interpulse coherence for the HS profile near 355 THz, likely due to its higher peak power under the same pulse duration. Yet the maximum value of interpulse coherence remains below 0.078, still far from unity. These consistently low coherence values reaffirm the effectiveness of the random-phase method in producing partially coherent pulse ensembles.

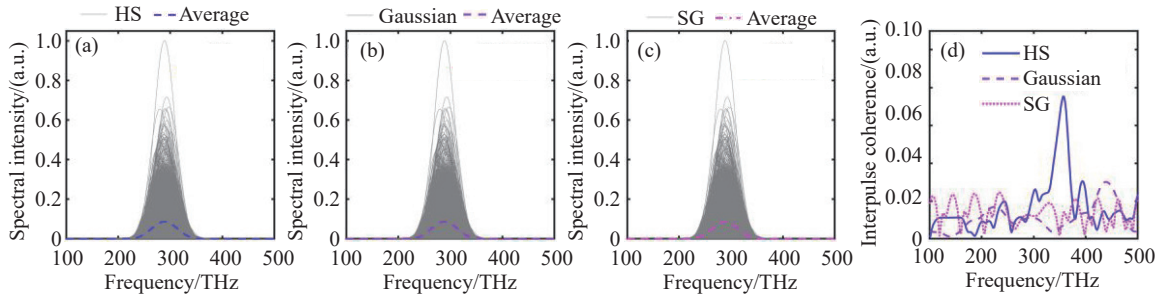


Fig. 2 Partially coherent pulse trains generated with initial spectral shapes: (a) HS, (b) Gaussian, (c) SG. Gray curves: 6000 randomly generated pulses. Dashed lines: averaged spectral intensity (blue: HS, violet: Gaussian, magenta: SG). (d) Interpulse coherence for HS (blue solid), Gaussian (violet dashed), and SG (magenta dotted).

## 2.2 Dispersion scan and differential evolution algorithm

D-scan is a pulse characterization technique

that exploits the high dispersion sensitivity of broadband ultrashort pulses. By systematically varying the dispersion introduced, for example, through a

pair of glass wedges, a two-dimensional trace is recorded by measuring the spectrum of the second-harmonic generation signal as a function of added dispersion. The second-harmonic signal can be expressed as the autoconvolution of the complex spectral field, similar in form to traces obtained in frequency-resolved optical gating. Retrieval of the pulse properties from the trace relies on an iterative phase-retrieval algorithm. In this work, we employ a DE algorithm for all reconstructions. The measured d-scan trace intensity  $I_d$  is given by

$$I_d = \left| \iint E(\omega') \exp[i\beta(\omega')z + i\omega't] d\omega' \exp(-i\omega t) dt \right|^2, \quad (2)$$

where  $z$  denotes the thickness of the dispersive material inserted (here BK7 glass), and  $\beta(\omega)$  is the corresponding propagation constant. The dispersion imposed on the pulse can be expanded as a Taylor series around the central frequency  $\omega_0$ :

$$\beta(\omega) = \beta_0 + \beta_1(\omega - \omega_0) + \frac{1}{2}\beta_2(\omega - \omega_0)^2 + \dots \quad (3)$$

where  $\beta_0$  and  $\beta_1$  affect only the absolute phase and group delay, respectively. For d-scan retrieval, the dominant term is the group-delay dispersion, represented by  $\beta_2$ . A key advantage of d-scan is its single-beam geometry, which avoids spatial-averaging artifacts and allows tight focusing for detection of weak pulses. While phase-matching bandwidth in the nonlinear crystal generally limits the measurable spectral range, this constraint can be circumvented by using Kerr-based nonlinearities that do not involve frequency conversion. In most implementations, however, dispersion is varied mechanically (e.g., translating wedges or grating pairs) on a timescale much slower than the laser repetition rate. Consequently, the recorded trace represents an average over many pulses, making the technique inherently susceptible to effects of partial coherence or pulse-train instability.

DE algorithm, introduced by Storn and Price in 1997, is a heuristic optimization algorithm inspired by evolutionary principles<sup>[30]</sup>. As a member of the

evolutionary-algorithm family, it searches for an optimum through successive generations of mutation, crossover, and selection within a population of candidate solutions. Unlike genetic algorithms that operate on binary strings, DE is designed for continuous parameter spaces, representing each individual as a vector of real-valued genes. The algorithm starts by initializing a population of random candidate solutions. In each generation, a mutant vector is created for every population member by adding a scaled difference between two other randomly selected individuals to a third distinct member. This differential mutation gives the method its name. The mutant then undergoes crossover with the original individual to produce an offspring. The fitness of each offspring is evaluated using a cost function, i.e., the discrepancy between the measured and simulated d-scan trace. Finally, a selection step retains the fitter individual between parent and offspring, maintaining a constant population size. This cycle repeats until convergence to an optimal solution.

To handle partially coherent pulse trains, we extend the standard DE approach by introducing an improved DE algorithm that retrieves multiple representative pulses simultaneously from a single averaged trace. Instead of seeking one deterministic field, the algorithm operates on an arbitrary subset of the ensemble, effectively reconstructing a statistical description of the fluctuating source. As the subset size increases, the retrieved ensemble better approximates the true stochastic behavior, at the cost of higher computational demand. In our simulations, we use 15 representative subsets to reconstruct the averaged d-scan trace. Although the improved algorithm requires more computational resources, its operations are parallelizable, offering a pathway for accelerated execution on parallel computing architectures.

### 3 Simulation results and discussions

In this section, we present simulation results

obtained using both the traditional and improved DE algorithms. For each algorithm, two cases are examined: variation in spectral width and variation in spectral shape. Our additional simulation show that the DE algorithm works well for the fully coherent pulse train.

### 3.1 Different initial spectral widths

Figure 3 illustrates three randomly selected sample pulses from the generated ensembles, validating the random-phase method used to produce partially coherent pulse trains. Compared with the interpulse coherence values shown in Figs. 1(d) and 2(d), these individual samples reveal richer details in amplitude and phase. For narrower spectra

[30 THz, Fig. 3(a1–a3)], fluctuations are less pronounced than for broader spectra [60 THz, Fig. 3(b1–b3); 100 THz, Fig. 3(c1–c3)]. The broader spectra exhibit stronger modulations, especially near the leading and trailing edges. Despite these fluctuations, the ensemble-averaged spectral and temporal profiles retain the initial Gaussian shape. Retrieved spectral amplitudes and phases are well defined for all three bandwidths [Figs. 3(a4–a5), 3(b4–b5), 3(c4–c5)]. Notably, while the spectral width increases with initial bandwidth, the temporal duration remains nearly constant, confirming that the pulse train is not Fourier-transform limited.

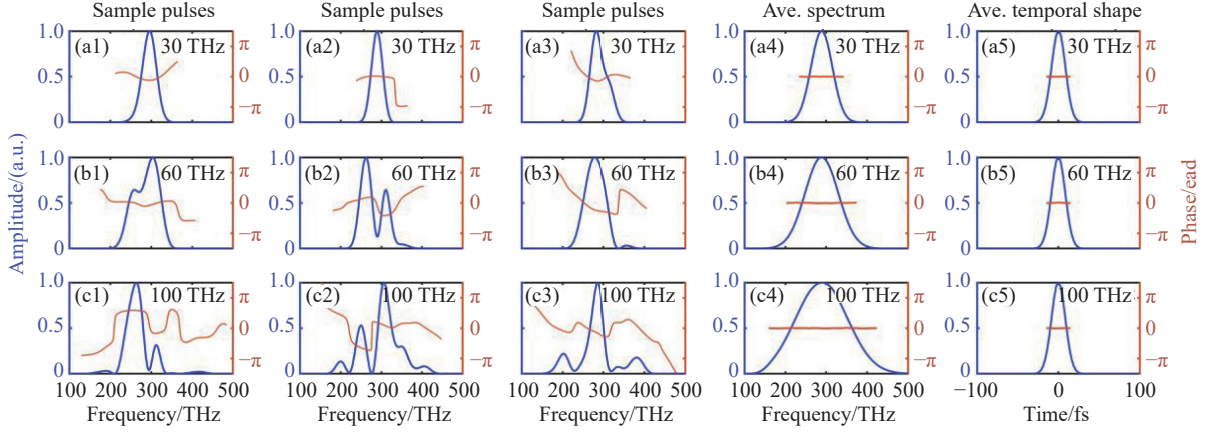


Fig. 3 Sample pulses for initial spectral width of (a1–a3) 30 THz, (b1–b3) 60 THz, and (c1–c3) 100 THz. (a4, b4, c4) Ensemble-averaged spectra; (a5, b5, c5) ensemble-averaged temporal shapes over 6000 pulses.

The average d-scan traces for fully coherent pulse trains are shown in Figs. 4(a1), 4(b1), and 4(c1) for 30 THz, 60 THz, and 100 THz, respectively. The corresponding traces retrieved with the traditional DE algorithm are displayed in Figs. 4(a2), 4(b2), and 4(c2). The traditional DE algorithm clearly distinguishes between fully coherent and partially coherent pulse trains. To quantify the discrepancy between the average and retrieved traces, we define the error metric[31]:

$$G = \sqrt{\frac{1}{M_i N_j} \sum_{i=1, j=1}^{i=M, j=N} [I_{\text{ave}}(\omega_i, z_j) - \alpha I_{\text{ret}}(\omega_i, z_j)]^2}, \quad (4)$$

where  $M$  and  $N$  are grid numbers for the frequency

and spatial windows,  $I_{\text{ave}}$  and  $I_{\text{ret}}$  are the average and retrieved d-scan intensities, and  $\alpha$  is the normalizing constant. Significant  $G$  values are observed for all spectral widths, confirming that traditional DE fails to accurately reconstruct the pulse ensemble. It primarily serves as a detector of coherence loss. For 30 THz, 60 THz, and 100 THz, the respective  $G$  values are 1.5% [Figs. 4(a1–a2)], 3.8% [Figs. 4(b1–b2)], and 6.7% [Figs. 4(c1–c2)]. Given the Fourier-transform-limited durations of 23.4 fs (30 THz), 11.7 fs (60 THz), and 7 fs (100 THz), these results indicate that retrieval becomes more challenging for shorter pulses.

To enhance retrieval accuracy, we employ the improved DE algorithm described in Section 2.2.

Figures 5(a)-(c) show the retrieved d-scan traces for 30 THz, 60 THz, and 100 THz, with  $G$  values reduced to 0.5%, 0.6%, and 0.8%, respectively. The lower error confirms that the improved algorithm yields significantly better reconstructions. The same trend of increasing  $G$  with bandwidth persists, consistent with the results in Fig. 4. The six traces plotted to the right of each panel in Fig. 5 represent selected subset traces. Individually, these traces deviate from the ideal reconstruction. However, their col-

lective average closely matches the ensemble-averaged d-scan trace. Each d-scan trace among the six d-scan traces are not unique. The non-uniqueness of the subset reflects the inherent variability in amplitude and phase across the partially coherent ensemble, running the algorithm again produces a different set of representative traces. The scenarios for 60 and 100 THz are the same as 30 THz, as shown in Figs. 5(b) and 5(c).

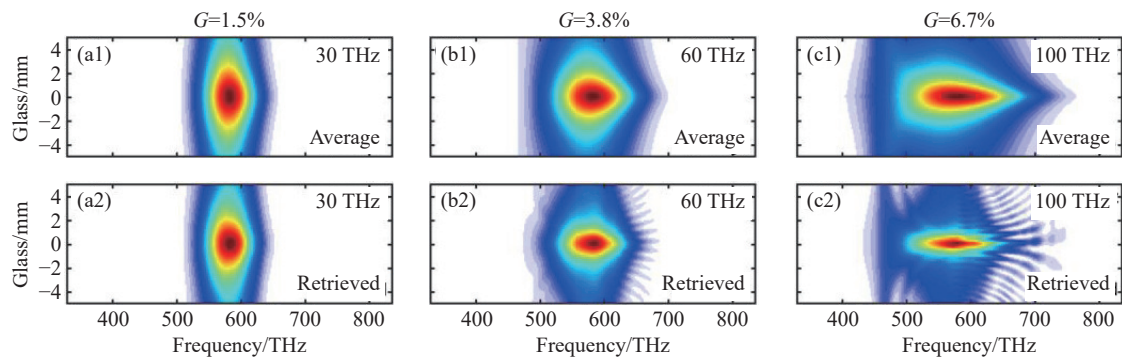


Fig. 4 (a1, b1, c1) Average d-scan traces for 30 THz, 60 THz, and 100 THz. (a2, b2, c2) Corresponding traces retrieved with traditional DE.

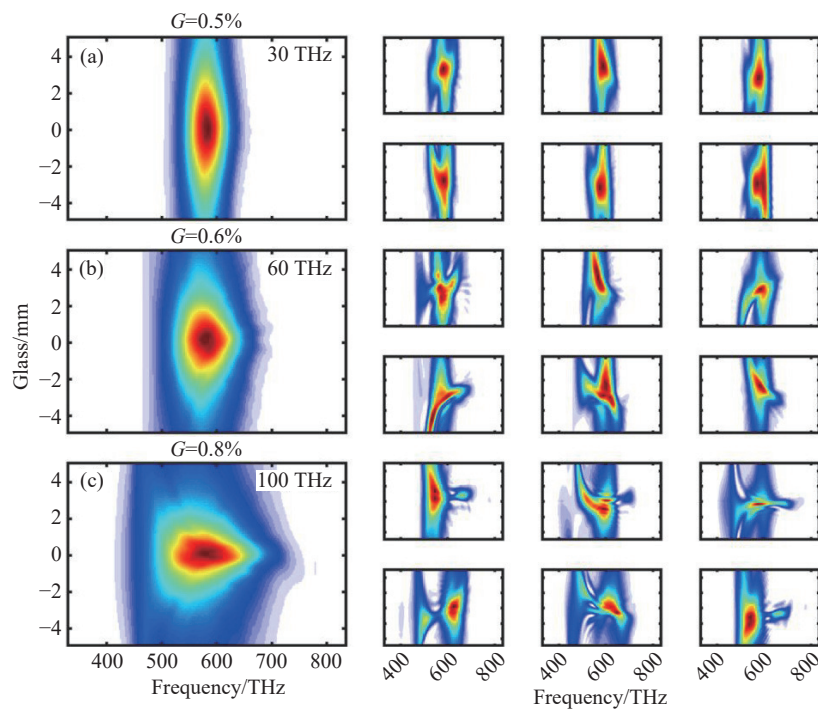


Fig. 5 Retrieved d-scan traces for (a) 30 THz, (b) 60 THz, and (c) 100 THz. Six representative subset traces are shown to the right of each panel.

Using the information extracted via the improved DE algorithm, we can reconstruct the statist-

ical properties of the entire ensemble. Figures 6 (a1–a3) display retrieved spectral waveforms for

30 THz, exhibiting complex and distinct amplitude-phase structures. Compared with the original sample pulses, the retrieved average spectra and temporal shapes are smoother, and their spectral phases approach zero. This smoothing effect becomes more pronounced for broader spectra [60 THz, Figs. 6 (b1–b5); 100 THz, Figs. 6(c1–c5)]. The near-zero phase indicates retrieval of nearly Fourier-transform-limited spectra. Comparing the retrieved aver-

age spectra in Figs. 6(a4), 6(b4), and 6(c4) with those in Figs. 3(a4), 3(b4), and 3(c4) shows that the retrieved spectral width increases with the initial bandwidth, while the temporal duration remains largely unchanged. This behavior mirrors the trend observed in Fig. 3, confirming that the improved DE algorithm successfully retrieves the statistical features of partially coherent pulse trains.

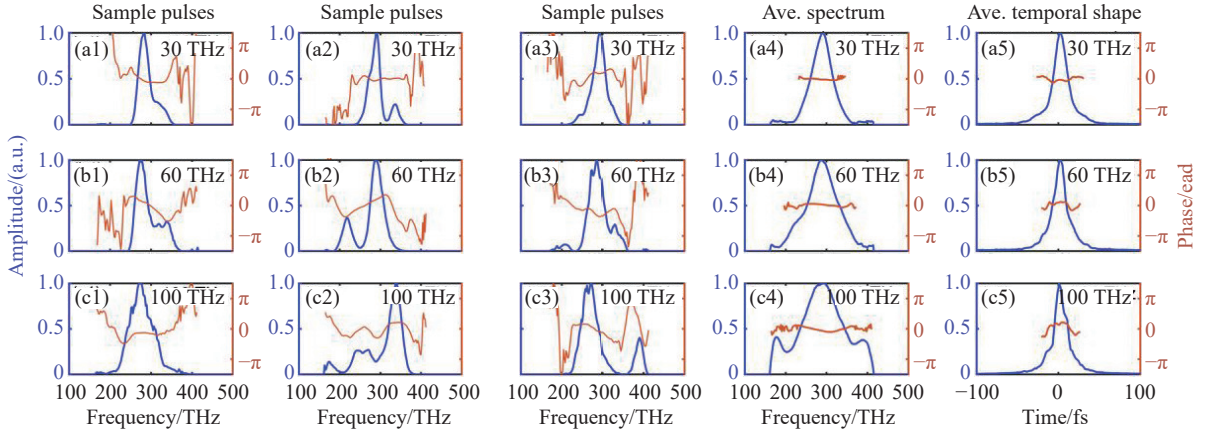


Fig. 6 Retrieved results for initial spectral width of (a1–a5) 30 THz, (b1–b5) 60 THz, and (c1–c5) 100 THz. (a1–a3, b1–b3, c1–c3) Random sample pulses; (a4, b4, c4) retrieved average spectrum and phase; (a5, b5, c5) retrieved average temporal shape and phase.

### 3.2 Different initial spectral shapes

We now apply the same analysis procedure described in Section 3.1 to different initial spectral shapes, namely HS, Gaussian, and SG. These functions are expressed as:

$$A_0(\omega) = \begin{cases} \operatorname{sech}\left[2\ln(1+\sqrt{2})(f-f_0)/\Delta f_{\text{FWHM}}\right] \\ \exp\left[-4\ln 2(f-f_0)^2/\Delta f_{\text{FWHM}}^2\right] \\ \exp\left[-16\ln 2(f-f_0)^4/\Delta f_{\text{FWHM}}^2\right] \end{cases}, \quad (5)$$

where  $f_0 = c/\lambda_0$  is the central frequency (with pump wavelength  $\lambda_0 = 1030$  nm and  $c$  the speed of light), and  $\Delta f_{\text{FWHM}}$  denotes the FWHM of the amplitude spectrum. Among the three profiles, HS exhibits the steepest rising and falling edges, Gaussian follows. SG, despite its steeper edges, has a flatter top and leading to a slower overall power variation. This difference likely explains why sample pulses for HS [Fig. 7(a1–a3)] show more pronounced fluctuations compared with Gaussian [Fig. 7(b1–b3)] and SG

[Fig. 7(c1–c3)]. The ensemble-averaged spectra and temporal shapes, displayed in Fig. 7(a4–a5) (HS), 7(b4–b5) (Gaussian), and 7(c4–c5) (SG), are smooth for all shapes, confirming that our generation method effectively produces partially coherent pulse trains across diverse spectral profiles.

We next apply the traditional DE algorithm to retrieve the d-scan traces and compare them with the directly averaged ensemble traces (Fig. 8). The resulting error values  $G$  defined in Eq. (4) are 7% for HS [Figs. 8(a1–a2)], 2.5% for Gaussian [Figs. 8(b1–b2)], and 1.9% for SG [Figs. 8(c1–c2)]. These errors are nearly equal to those observed for different spectral widths, indicating that traditional DE fails to accurately reconstruct the d-scan trace for partially coherent pulse trains. While broader spectra increase retrieval difficulty in the width-variation case, the shape-variation case shows that profiles with faster amplitude changes pose greater

challenges. HS, with its steep edges, is the most difficult to retrieve. This is particularly relevant be-

cause HS profiles are commonly encountered in commercial mode-locked laser outputs.

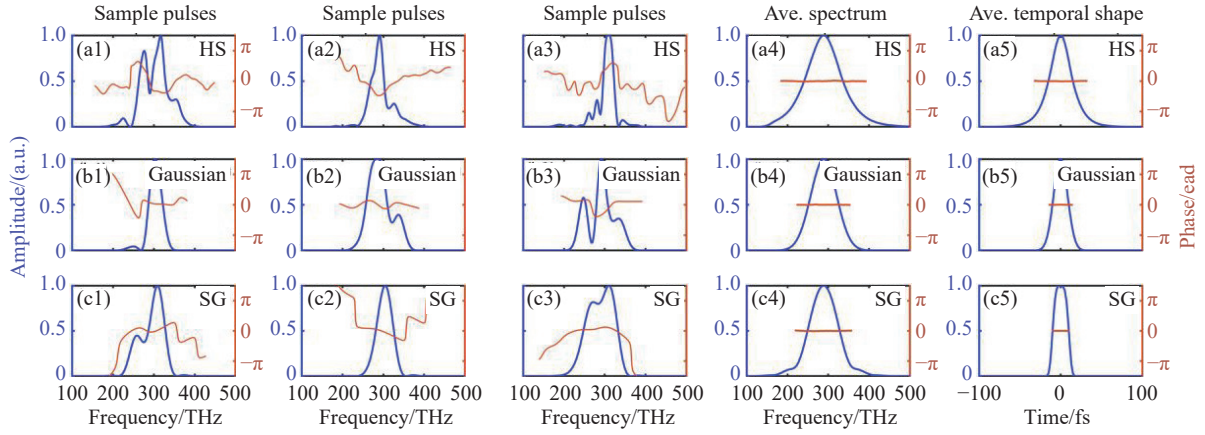


Fig. 7 Sample pulses for initial spectral shape and phase of (a1–a3) HS, (b1–b3) Gaussian, and (c1–c3) SG. (a4, b4, c4) Ensemble-averaged spectra and phase; (a5, b5, c5) ensemble-averaged temporal shapes and phase.

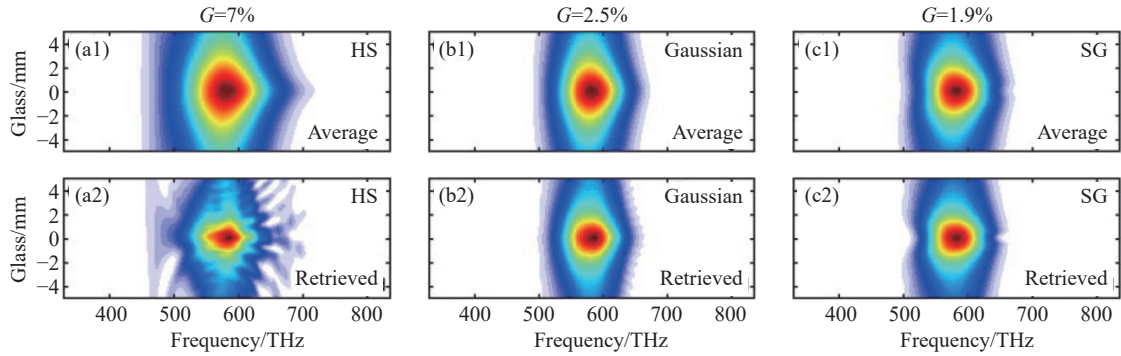


Fig. 8 (a1, b1, c1) Average d-scan traces for HS, Gaussian, and SG. (a2, b2, c2) Corresponding traces retrieved with traditional DE.

We now employ the improved DE algorithm to retrieve the traces for different spectral shapes (Fig. 9). The error values are reduced to 1% for HS [Fig. 9(a)], 0.6% for Gaussian [Fig. 9(b)], and 0.5% for SG [Fig. 9(c)], confirming that the improved algorithm yields significantly better reconstructions. The same trend that HS being the most challenging persists, but the improved algorithm offers an additional advantage. It can retrieve subsets of the ensemble, as illustrated by the six representative traces plotted to the right of each panel. While individual subset traces are not unique (reflecting the stochastic nature of the source), their statistical aggregation enables robust retrieval based on ensemble averaged patterns.

Finally, we present the retrieved spectral and temporal waveforms based on the improved DE results (Fig. 10). Sample pulses for HS [Figs. 10(a1–a3)] exhibit slightly more pronounced pedestals compared with Gaussian [Figs. 10(b1–b3)] and SG [Figs. 10(c1–c3)]. Nevertheless, smooth average spectra and temporal shapes are obtained for all three profiles. The close agreement between the retrieved averages in Fig. 10 and the original ensemble averages in Fig. 7 validates the effectiveness of the improved algorithm. A careful comparison reveals that the retrieved average spectra and temporal shapes for HS [Figs. 10(a4–a5)] retain slightly more residual fluctuations than those for Gaussian [Figs. 10(b4–b5)] and SG [Figs. 10(c4–

c5)], reinforcing the observation that HS remains the most difficult profile to retrieve among the three shapes considered.

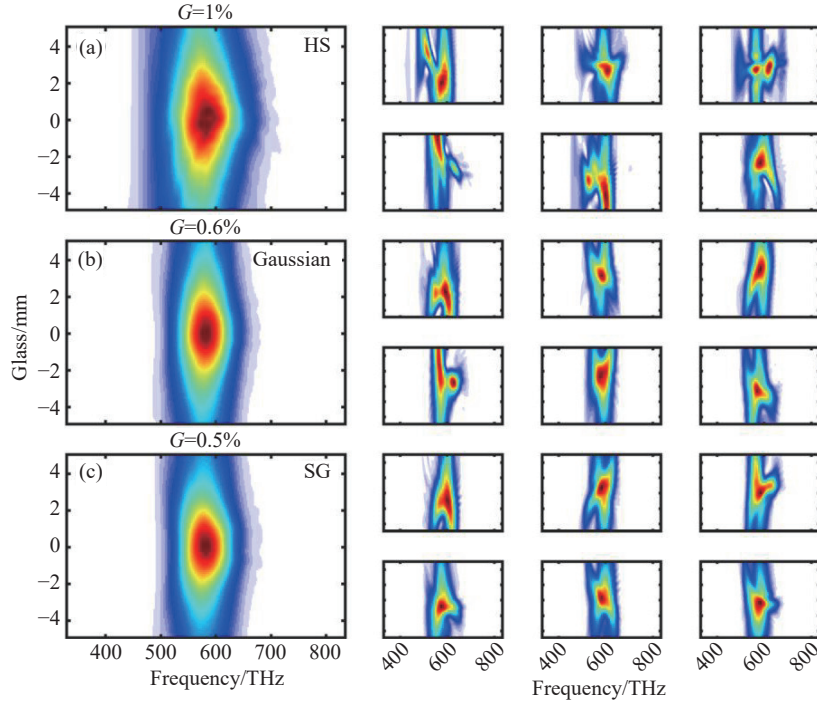


Fig. 9 Retrieved d-scan traces for (a) HS, (b) Gaussian, and (c) SG. Six representative subset traces are shown to the right of each panel.

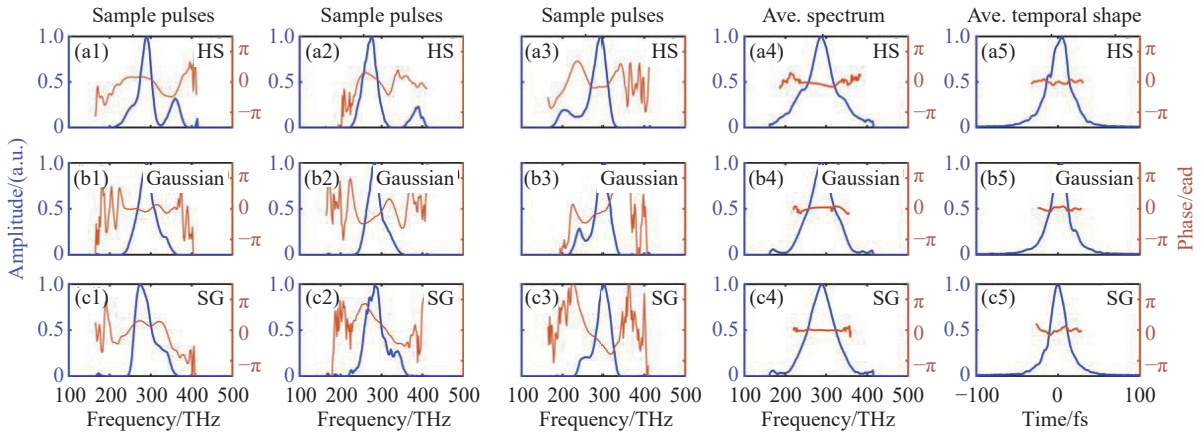


Fig. 10 Retrieved results for initial spectral shape of (a1–a5) HS, (b1–b5) Gaussian, and (c1–c5) SG. (a1–a3, b1–b3, c1–c3) Random sample pulses; (a4, b4, c4) retrieved average spectrum and phase; (a5, b5, c5) retrieved average temporal shape and phase.

## 4 Conclusion

In this study, we first generated partially coherent pulse trains using the random-phase method. The calculated interpulse coherence, which remains well below unity, confirms the stochastic nature of

the generated ensemble. These partially coherent pulse trains were subsequently characterized via d-scan under two distinct scenarios: variations in spectral width and variations in spectral shape. The traditional DE algorithm proved inadequate for retrieving the average d-scan trace of a partially coherent pulse train. For the spectral-width case, the retrieval

error increases with bandwidth, reaching a maximum G value of 6.7% at 100 THz. Similarly, in the spectral-shape case, the largest error (7%) occurs for the HS profile. In contrast, the improved DE algorithm substantially reduces these errors, yielding maximum G-values of 0.8% (spectral-width variation) and 1% (spectral-shape variation).

In summary, by combining the respective strengths of the two DE variants, we demonstrate

that DE can not only discriminate between coherent and partially coherent pulse trains, but also accurately retrieve the average d-scan trace of a partially coherent ensemble. Crucially, the improved DE algorithm enables reconstruction from subsets of the ensemble, extending its applicability to the most general experimental conditions in which full ensemble information may be unavailable or impractical to acquire.

## References:

- [1] STRICKLAND D, MOUROU G. Chirped pulse amplification[J]. *Optics Communications*, 1985, 56(3): 219-221.
- [2] TREBINO R, DELONG K W, FITTINGHOFF D N, *et al.*. Measuring ultrashort laser pulses in the time-frequency domain using frequency-resolved optical gating[J]. *Review of Scientific Instruments*, 1997, 68(9): 3277-3295.
- [3] HUANG SH W, CIRMI G, MOSES J, *et al.*. High-energy pulse synthesis with sub-cycle waveform control for strong-field physics[J]. *Nature Photonics*, 2011, 5(8): 475-479.
- [4] 冷雨欣. 从啁啾脉冲放大到强场激光物理——2018年诺贝尔物理学奖解读[J]. *自然杂志*, 2018, 40(6): 400-406.  
LENG Y X. From chirped pulse amplification to high field laser physics: a brief introduction to the Nobel Prize in Physics 2018[J]. *Chinese Journal of Nature*, 2018, 40(6): 400-406. (in Chinese).
- [5] KIM M, LEE C, SHIN P, *et al.*. Generation of 1 MHz 15 fs pulses in the near-infrared with high energy and their application to time-resolved spectroscopy[J]. *Optics Express*, 2024, 32(21): 36577-36585.
- [6] KIM J. Practical method for achieving single-photon femtosecond time-resolved spectroscopy: transient stimulated emission[J]. *The Journal of Physical Chemistry Letters*, 2024, 15(20): 5407-5412.
- [7] OKSENHENDLER T, BOCK S, DREYER J, *et al.*. Advanced laser pulse metrology through 2D self-referenced spectral interferometry[J]. *Scientific Reports*, 2025, 15(1): 17729.
- [8] KANG Y, WANG X H, TANG L H, *et al.*. High repetition rate and high energy ultrashort laser pulse: the next light source for attosecond spectroscopy[J]. *ACS Photonics*, 2025, 12(5): 2279-2290.
- [9] TORRES-COMPANY V, LAJUNEN H, FRIBERG A T. Coherence theory of noise in ultrashort-pulse trains[J]. *Journal of the Optical Society of America B*, 2007, 24(7): 1441-1450.
- [10] YANG Y T, JI Y B, XIE Y H, *et al.*. Generation and observation of noise-like pulses in an ultrafast fiber laser at 1.7  $\mu\text{m}$ [J]. *Optics & Laser Technology*, 2024, 174: 110715.
- [11] WANG ZH H, ZHOU Z X, JI Y B, *et al.*. Dynamic observation of ultrashort pulses with chaotic features in a tm-doped fiber laser with a single mode fiber-grade index multimode fiber-single mode fiber structure[J]. *Photonics*, 2025, 12(5): 465.
- [12] BERMÚDEZ MACIAS I J, DÜSTERER S, IVANOV R, *et al.*. Study of temporal, spectral, arrival time and energy fluctuations of SASE FEL pulses[J]. *Optics Express*, 2021, 29(7): 10491-10508.
- [13] SOCOL Y, GOVER A, ELIRAN A, *et al.*. Study of coherence limits and chirp control in long pulse FEL oscillator[J]. *Physical Review Special Topics-Accelerators and Beams*, 2005, 8: 080701.
- [14] KOVALSKY M G, HNILO A A, TREDICCE J R. Extreme events in the Ti: sapphire laser[J]. *Optics Letters*, 2011, 36(22): 4449-4451.
- [15] TANG ZH Q, LUO D P, XIE G H, *et al.*. Nonlinear dynamics of relative intensity noise transfer at fiber amplification and supercontinuum generation[J]. *Optics Communications*, 2024, 554: 130131.
- [16] SIMPSON T B, SUELZER J S, USECHAK N G. Phase shifts in gain-switched semiconductor laser subharmonic pulse trains[J]. *IEEE Journal of Quantum Electronics*, 2024, 60(6): 2000512.
- [17] BASAK S, BLANCO A, LÓPEZ C. Large fluctuations at the lasing threshold of solid-and liquid-state dye lasers[J]. *Scientific Reports*, 2016, 6: 32134.
- [18] ANGELSKY O V, BEKSHAEV A Y, ZENKOVA C Y, *et al.*. Correlation optics, coherence and optical singularities:

- basic concepts and practical applications[J]. *Frontiers in Physics*, 2022, 10: 924508.
- [19] POLLI D, BRIDA D, MUKAMEL S, *et al.*. Effective temporal resolution in pump-probe spectroscopy with strongly chirped pulses[J]. *Physical Review A*, 2010, 82(5): 053809.
- [20] RHODES M, STEINMEYER G, RATNER J, *et al.*. Pulse - shape instabilities and their measurement[J]. *Laser & Photonics Reviews*, 2013, 7(4): 557-565.
- [21] SYTCEVICH I, GUO CH, MIKAELSSON S, *et al.*. Characterizing ultrashort laser pulses with second harmonic dispersion scans[J]. *Journal of the Optical Society of America B*, 2021, 38(5): 1546-1555.
- [22] TAJALLI A, CHANTEAU B, KRETSCHMAR M, *et al.*. Few-cycle optical pulse characterization via cross-polarized wave generation dispersion scan technique[J]. *Optics Letters*, 2016, 41(22): 5246-5249.
- [23] SALGADO-REMACHA F J, ALONSO B, CRESPO H, *et al.*. Single-shot d-scan technique for ultrashort laser pulse characterization using transverse second-harmonic generation in random nonlinear crystals[J]. *Optics Letters*, 2020, 45(14): 3925-3928.
- [24] MIRANDA M, ARNOLD C L, FORDELL T, *et al.*. Characterization of broadband few-cycle laser pulses with the d-scan technique[J]. *Optics Express*, 2012, 20(17): 18732-18743.
- [25] KLEINERT S, TAJALLI A, NAGY T, *et al.*. Rapid phase retrieval of ultrashort pulses from dispersion scan traces using deep neural networks[J]. *Optics Letters*, 2019, 44(4): 979-982.
- [26] GERTH D, ESCOTO E, STEINMEYER G, *et al.*. Regularized differential evolution for a blind phase retrieval problem in ultrashort laser pulse characterization[J]. *Review of Scientific Instruments*, 2019, 90(4): 043116.
- [27] KOROBEENKO A, ROSENBERGER P, SCHÖTZ J, *et al.*. Single-shot dispersion sampling for optical pulse reconstruction[J]. *Optics Express*, 2021, 29(8): 11845-11853.
- [28] PFEIFER T, JIANG Y H, DÜSTERER S, *et al.*. Partial-coherence method to model experimental free-electron laser pulse statistics[J]. *Optics Letters*, 2010, 35(20): 3441-3443.
- [29] DUDLEY J M, GENTY G, COEN S. Supercontinuum generation in photonic crystal fiber[J]. *Reviews of Modern Physics*, 2006, 78(4): 1135-1184.
- [30] STORN R, PRICE K. Differential evolution—a simple and efficient heuristic for global optimization over continuous spaces[J]. *Journal of Global Optimization*, 1997, 11(4): 341-359.
- [31] ESCOTO E, GERTH D, HOFMANN B, *et al.*. Strategies for the characterization of partially coherent ultrashort pulses with dispersion scan[J]. *Journal of the Optical Society of America B*, 2019, 36(8): 2092-2098.

#### Author Biographies:



YIN Chen (2002—), B.S., Department of Physics, School of Physical Science and Technology, Ningbo University. His research interests are the generation and measurement of ultrashort pulses. E-mail: [2511690141@nbu.edu.cn](mailto:2511690141@nbu.edu.cn)



YANG Pei-long (1987—), Ph.D., Professor, Laboratory of Infrared Materials and Devices, The Research Institute of Advanced Technologies, Ningbo University. His research interests are mid-infrared ultrafast lasers, nonlinear fiber optics, and mid-infrared supercontinuum generation in soft-glass fibers. E-mail: [yangpeilong@nbu.edu.cn](mailto:yangpeilong@nbu.edu.cn)



MEI Chao (1989—), Ph.D., Professor, Department of Physics, School of Physical Science and Technology, Ningbo University. His research interests include nonlinear optics, strong-field optics, and nonlinear dynamics in optical devices and lasers. E-mail: [meichao@nbu.edu.cn](mailto:meichao@nbu.edu.cn)